A R C H I V E S O F M E T A L L U R G Y A N D M A T E R I A L S
Volume 60 2015 Issue 2
DOI: 10.1515/amm-2015-0155

S.A. SONG*, M.J. LIM**, K.Y. JUNG**,♯, W.-W. SO***, S.-J. MOON***

IMPROVED LIGHT CONVERSION EFFICIENCY OF DYE-SENSITIZED SOLAR CELL BY DISPERSING SUBMICRON-SIZED GRANULES INTO THE NANO-SIZED TiO_2 LAYER

POPRAWA EFEKTYWNOŚCI KONWERSJI ŚWIATŁA OGNIW SŁONECZNYCH UCZULONYCH BARWNIKIEM POPRZEZ ROZPROSZENIE SUBMIKRONOWYCH GRANULEK W WARSTWIE NANOCZĄSTEK TiO_2

In this work, TiO_2 nanoparticles and submicron-sized granules were synthesized by a hydrothermal method and spray pyrolysis, respectively. Submicron-sized granules were dispersed into the nano-sized TiO_2 layer to improve the light conversion efficiency. Granules showed better light scattering, but lower in terms of the dye-loading quantity and recombination resistance compared with nanoparticles. Consequently, the nano-sized TiO_2 layer had higher cell efficiency than the granulized TiO_2 layer. When dispersed granules into the nanoparticle layer, the light scattering was enhanced without the loss of dye-loading quantities. The dispersion of granulized TiO_2 led to increase the cell efficiency up to 6.51%, which was about 5.2 % higher than that of the electrode consisting of only TiO_2 nanoparticles. Finally, the optimal hydrothermal temperature and dispersing quantity of granules were found to be 200°C and 20 wt%, respectively.

Keywords: Titania nanoparticles, Granules, Dye-sensitized solar cell, Light scattering, Spray pyrolysis

1. Introduction

Dye-sensitized solar cells (DSSCs) are considered as one of the potential solar cells due to their low fabrication cost and simple structure compared with conventional silicon solar cells [1-2]. The light-conversion efficiency of DSSCs, however, is low and needed to be increased for successful commercialization. For past two decades, therefore, a lot of researches have been focused on the improvement of the cell efficiency through developing new anode materials, dyes and electrolytes [3-7].

Nano-sized TiO_2 has been used as the anode materials of DSSCs due to its suitable band structure for dye molecules, good photo-chemical stability and large surface area [8-11]. Basically, the photo-conversion efficiency of DSSCs depends on the light-harvesting efficiency of dye molecules and how to effectively extract the photo-excited electrons out of the photoanode. Photoelectrodes consisting of nanoparticles should have high surface area for the large uptake of dye molecules, and effectively harvest the incoming light. For a typical porous thin-film anode, the higher in the light scattering the better in the light harvesting of dye molecules. Also, a good interconnection between TiO_2 nanoparticles plays a key role on the increase of the cell efficiency because it is related strongly with the extraction rate of photo-excited electrons as well as the recombination resistance of photoanodes [12-13]. In terms of the light scattering, titania particles with submicron size is better than nanoparticles [14-15]. But, the large particle size is not good for the interconnection in photoanodes.

To improve the light-conversion efficiency of DSSCs without an additional light-scattering layer, in this work, the light scattering of nano-sized TiO_2 films was enhanced by dispersing submicron-sized TiO_2 granules. Anatase TiO_2 nanoparticles were prepared by a hydrothermal method and submicron-sized granules were prepared by spray pyrolysis using the synthesized nanoparticles. The effect of the dispersion quantity of granules on the photovoltaic performance of DSSCs was investigated systematically.

2. Materials and methods

Nano-sized TiO_2 particles were synthesized by a conventional hydrothermal method. In a typical procedure for the synthesis of anatase nanoparticles, a colloidal solution was first prepared by heating a mixture, comprising 50 mL of titanium isopropoxide (TTIP, 97%, Adlrich), 110 mL of acetic acid, 14 mL of isopropanol (IPA), at 80°C for 24 h. The added IPA was removed by using a rotary vacuum evaporator at 50°C. Next, the resulting colloidal solution was filled in a Teflon vessel after the total volume was adjusted to be 500 mL by adding water and followed by the hydrothermal treatment for 24 h at the temperature range from 160°C to 230°C. As-synthesized TiO_2 nanoparticles were withdrawn by filtration, followed by the drying in a vacuum oven at room temperature.

TiO_2 granules were prepared by a conventional spray pyrolysis process consisting of an aerosol generator with ultra-

* MICRO/NANO SCALE MANUFACTURING RESEARCH GROUP, KOREA INSTITUTE OF INDUSTRIAL TECHNOLOGY, ANSAN-SI, REPUBLIC OF KOREA
** DEPARTMENT OF CHEMICAL ENGINEERING, KONGJU NATIONAL UNIVERSITY, CHEONAN, REPUBLIC OF KOREA
*** ENERGY MATERIALS RESEARCH CENTER, KOREA RESEARCH INSTITUTE OF CHEMICAL TECHNOLOGY, DAEJEON, REPUBLIC OF KOREA
♯ Corresponding author: kyjung@kongju.ac.kr

sonic vibrator (1.7 MHz), a quartz reactor (1500 mm in length and 55 mm in diameter) and a Teflon bag filter. The colloidal spray solution (3 g/L) prepared by using the hydrothermal synthesized TiO_2 nanoparticles was atomized by the ultrasonic aerosol generator to produce many droplets which were carried by air (30 liter/min) into the quartz reactor at 900°C. The produced powder was collected by a bag filter and followed by the calcinations at 500°C for 4h. Titania paste was prepared by dispersing TiO_2 particles (0.5g) into in the mixture of α-terpinol (solvent, 1.5g) and ethyl cellulose (binder, 0.2g) using a centrifugal mixer (THINKY Co. ARM-310) for 30 min, and followed by a three-roll milling process. In this step, TiO_2 granules were mixed with nanoparticles and the weight fraction of granules was controlled to be 10, 20 and 30 wt%. To prepare the working electrode, a thin TiO_2 blocking layer was first formed on the FTO glass (1.4 cm ×0.8 cm) by immersing $TiCl_4$ aqueous solution (0.04 M) at room temperature, drying in a convection oven at 70°C for 20 min, and washing with ethanol. Thereafter, the TiO_2 past film was formed by a doctor-blade method and followed by the heat treatment at 550°C for 10 min. Dye impregnation was carried out by immersing the prepared TiO_2 anode in ethanol solution of N719 dye (0.25 mM) for 18 h at room temperature under excluding the outside light. The Pt counter electrode film was also prepared by the doctor-blade method using a Pt paste on the FTO glass in which two holes were drilled before making the Pt film. The prepared Pt paste film was calcined at 400°C (10°C /min) for 20 min. The dye-impregnated TiO_2 working electrode and Pt-counter electrode were assembled into a sandwich type cell by using the Surlyn sealant (DuPont, 60 μm thickness) which was melted on a hot plate at 180°C. A drop of electrolyte (EL-HSE, DYESOL) was injected into the hole made in the Pt-counter electrode. Finally, the holes were sealed by melting the Surlyn film with a soldering iron.

The particle size and morphology of synthesized TiO_2 nanoparticles or granules was measured by scanning electron microscopy (SEM, TESCAN, MIRA LHM) and transmission electron microscopy (TEM, JEOL, JEM1210). The BET surface area, pore size, and pore volume of prepared granules were obtained from the nitrogen adsorption-desorption isotherms measured by Micromeritics ASAP 2020. The change of crystallographic form was monitored by X-ray diffraction (XRD, RIGAGU RINT-2100) measurement. Diffused light scattering characteristics of the photoanodes before and after the dye loading were monitored by using a UV-vis spectrophotometer (Shimadzu, UV-2450). Photovoltaic performance of DSSCs was evaluated by measuring the current-voltage (J-V) characteristic curves using a solar simulator (McScience, K101 LAB20). The simulated light power was calibrated to one sun (100 mW/cm^2) using a reference Si photodiode. Electrochemical impedance spectroscopy measurements (AutoLAB, PGSTAT30) were performed at the open circuit voltage (Voc) bias with the frequency range from 0.01 Hz to 100 kHz.

3. Results and discussion

Figure 1 shows the TEM images of the as-prepared TiO_2 nanoparticles by hydrothermal treatment. The prepared TiO_2 nanoparticles have a rod-like shape and their size increases progressively from about 10 nm to 30 nm with increasing the hydrothermal temperature. Figure 2 shows the XRD patterns of the prepared nanoparticles. The observed peaks in the XRD patterns indicate anatase TiO_2 regardless of the hydrothermal temperature. A very weak peak for rutile was generated when the temperature was 230°C.

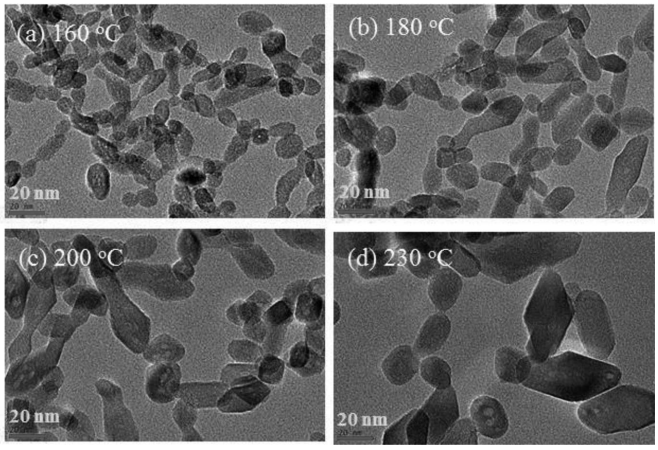

Fig. 1. TEM images of TiO_2 nanoparticles synthesized by a hydrothermal method at different temperaures

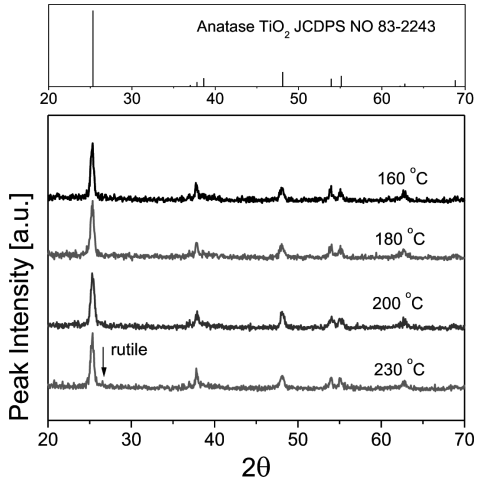

Fig. 2. XRD patterns of TiO_2 nanoparticles synthesized by a hydrothermal method at different temperaures

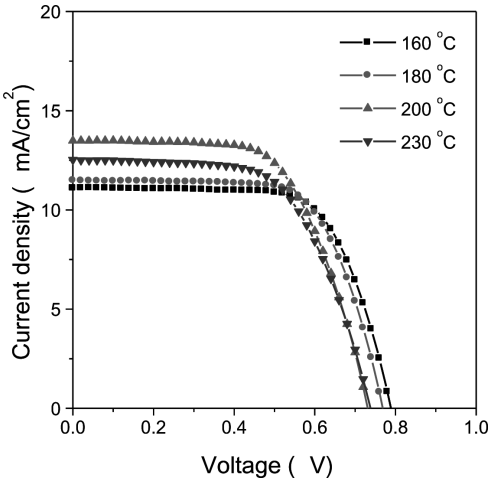

Fig. 3. I-V curves of DSSCs prepared using the hydrothermal-synthesized TiO_2 nanoparticles at different temperatures

The effect of hydrothermal temperature on the photovoltaic performance of DSSCs was investigated. Figure 3 shows the I-V curves of photoanodes prepared by using the hydrothermal-synthesized TiO_2 nanoparticles. The measured cell properties such as open-circuit voltage, current density, fill factor and efficiency were displayed in Fig. 4 as a function of the hydrothermal temperature. The current densities were 11.1, 11.5, 13.5 and 12.5 mA/cm^2 for 160, 180, 200 and 230°C, respectively. The values of open-circuit voltage and fill factor decreased monotonically as increasing the temperature. The measured cell efficiency increases with the hydrothermal temperature, and reaches the highest value of 6.2% at 200°C due to the increase of crystallinity. At 230°C, the lowest cell efficiency was achieved, which is due to the generation of rutile phase. Given these results, the optimal hydrothermal temperature was determined to be 200°C.

TiO_2 granules having submicron size were prepared using the nanoparticles which were prepared at the hydrothermal temperature of 200°C. Figure 5 a and b show SEM photos for nanoparticles prepared by the hydrothermal method and granular particles prepared by spray pyrolysis. The granules have spherical shape and average particle size of 400 nm as shown in Fig. 5 c. Figure 5 d shows the XRD patterns of granular particles, indicating that the prepared granules have pure anatase phase. That is, no phase transition from anatase to rutile occurs after the granulation process at 900°C. The pore properties of granulized TiO_2 particles were evaluated by using N_2 adsorption-desorption isotherms. Figure 5 e shows the measured adsorption-desorption isotherm, indicating that the granules have a type IV isotherm typically observed in mesoporous materials. The pore size distribution of granulized TiO_2 particles was shown in Fig. 5 f. A strong peak between 10 nm to 20 nm was observed. The BET surface area and the average pore size were 77 m^2/g and 13.1 nm, respectively.

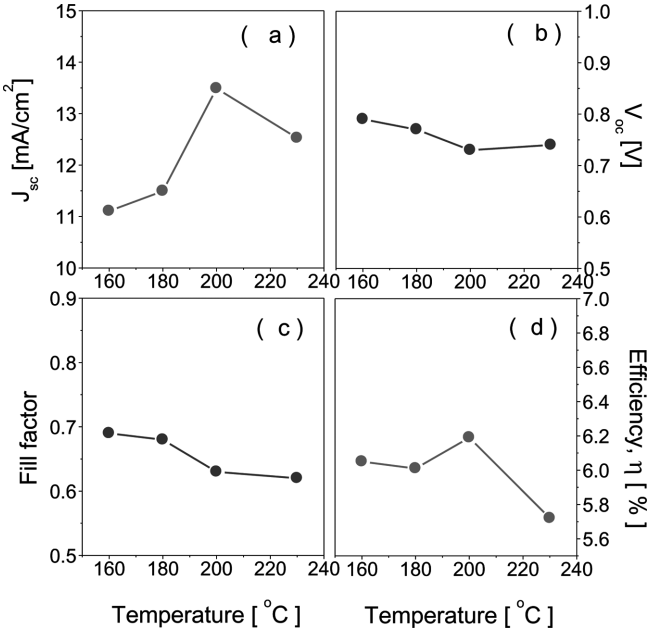

Fig. 4. Changes in current density (a), open-circuit voltage (b), fill factor (c), and efficiency (d) of DSSCS as a function of hydrothermal temperature

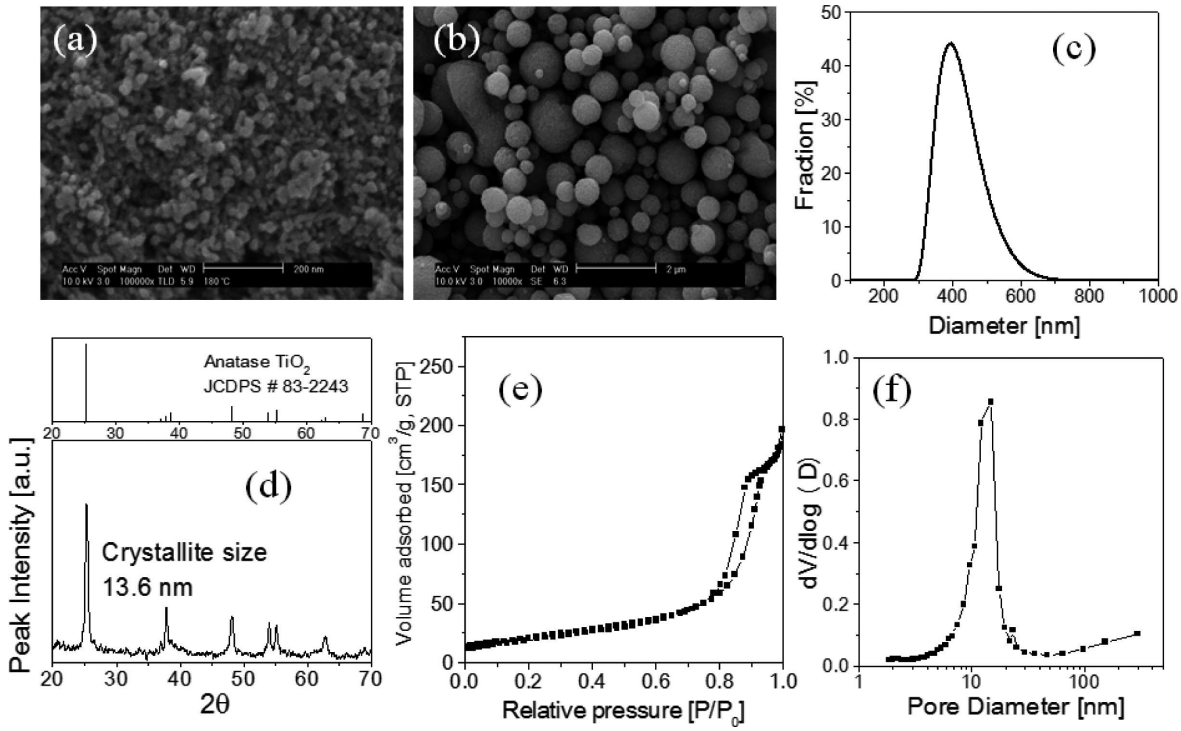

Fig. 5. SEM images of (a) nanoparticles and (b) granules. Particle size distribution (c), XRD pattern (d), N_2 adsorption-desorption isotherm (e) and pore size distribution (f) of TiO_2 granules

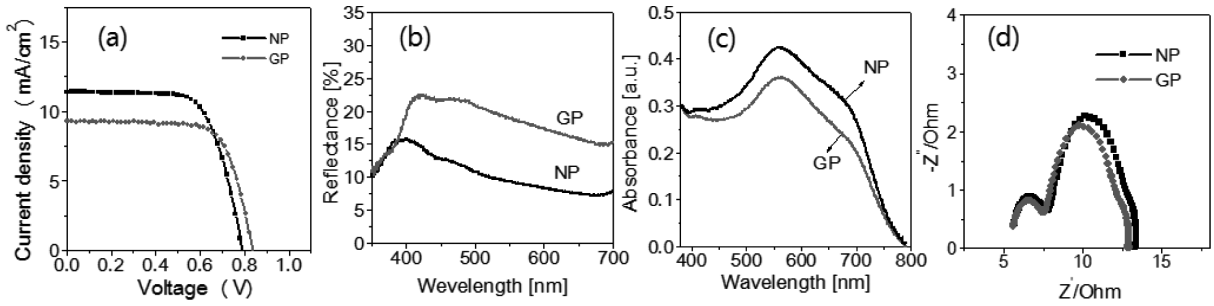

Fig. 6. (a) I-V curves, (b) UV/visible reflectance before the dye loading, (c) light absorbance after the dye loading, and (d) Nyquist plots of photoelectrodes prepared by using nanoparticles and granules

DSSC cells were fabricated by using nanoparticles synthesized by the hydrothermal method and granular particles prepared by spray pyrolysis. The current density-voltage (I-V) curves of the prepared photoanodes were measured under simulated 1.5 AM solar illumination, and the results were shown in Fig. 6 a. Detailed photovoltaic characteristics were summarized in TABLE 1. The observed current densities were 11.41 mA/cm^2 and 9.27 mA/cm^2 for NP- and GP-based photoanodes, respectively. As a result, the cell efficiency (η = 6.19%) of the NP-based photoanode is higher than that of the GP cell although the cell voltage and fill factor of the GP-based photoanode are a little larger compared with the NP-based photoanode.

TABLE 1
Photovoltaic parameters of the DSSCs prepared with changing anode materials

Anode Materials	GP content [wt%]	V_{oc}[V]	J_{sc}[mA/cm^2]	FF [%]	PCE [%]
NP	0	0.79	11.41	0.69	6.19
NP/GP	10	0.77	12.35	0.67	6.33
	20	0.77	12.36	0.68	6.51
	30	0.79	11.68	0.63	5.83
GP	100	0.84	9.27	0.72	5.60

The DSSC efficiency strongly depends on the light scattering of photoanodes, the loading quantity of dye molecules, and the charge transfer characteristics of TiO_2/dye/electrolyte interface. To investigate the light scattering properties of photoanodes fabricated with NP and GP, the diffuse reflectance of electrode films were measured before the dye loading. The resulting reflectance spectra were shown in Fig. 6 b. The anode film composed of mesoporous granules have higher diffuse reflectance capability compared with the film prepared using nanoparticles, indicating that the incident light can be more scattered within the GP film. The absorbance of photoanode films after the dye loading was shown in Fig. 6c. The NP film has higher absorbance than the GP film, which means that more dye loading is achieved in the NP film. Figure 6 d shows Nyquist plots of the electrochemical impedance spectroscopy (EIS) for the NP and GP films. Among three semicircles, the largest semicircle in the intermediate-frequency region is attributed to the charge transfer of TiO_2/dye/electrolyte interface. The width of the semicircle at the intermediate frequency is connected with the recombination resistance (R_{ct}). That is, the recombination rate in the GP film is larger than that in the NP film due to the weak connection between granules. From the results of diffuse reflectance, absorbance and EIS, the lower cell efficiency of the GP-based photoanode compared with the NP-based one is due to the small dye-loading quantity and low recombination resistance although the light scattering is larger.

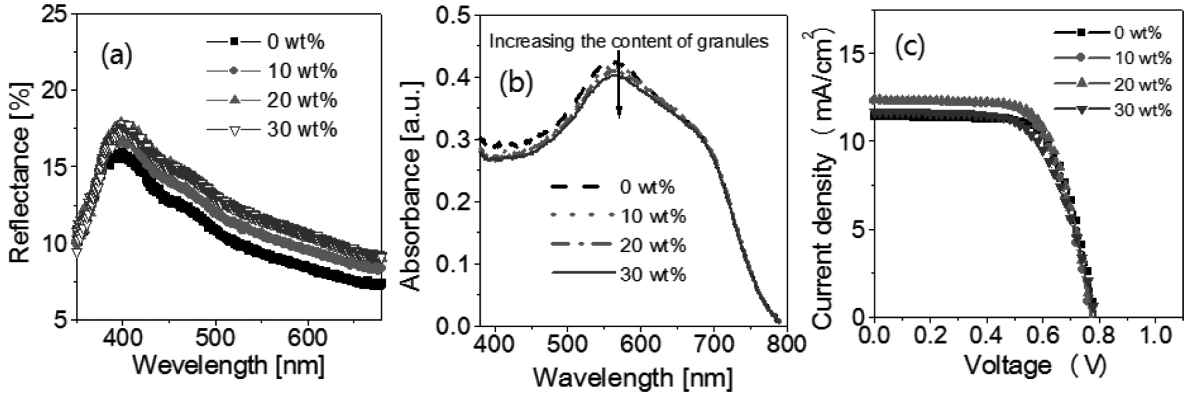

Fig. 7. (a) UV/visible reflectance, (b) light absorbance, and (c) I-V curves of photoelectrodes prepared by changing the GP fraction dispersed into the nano-sized TiO_2 anode film

To improve the light scattering of the NP film without the decrement in the dye loading, the granulized TiO_2 particles were dispersed into the nano-sized TiO_2 film. Figure 7 a and b show the diffuse reflectance and the absorbance of films prepared by changing the GP quantity before and after the dye loading, respectively. The dispersion of submicron granules into the nano-sized TiO_2 film enhances the light scattering. The absorbance of photoanode films after the dye loading indicates that there is no significant change in the loading quantity of dye molecules at the weight percentage of granules of 20 wt%. When the weight percentage of granules dispersed was 20% and larger, however, a little decrement in the dye loading was observed. Figure 7 c shows the I-V curves of the photoanodes with changing the dispersion quantity of submicron TiO_2 granules. Detailed photovoltaic characteristics as varying the dispersion quantity of granules were summarized in TABLE 1. When the dispersion quantities were 10, 20 and 30 wt%, the current densities was 12.35, 12.36 and 11.68 mA/cm^2, respectively. Compared with the cell prepared by using only nano-sized TiO_2, the dispersion of submicron granules led to improve the current density. There was no significant change in the cell voltage as changing the quantity of granules dispersed. As a result, the dispersion of submicron TiO_2 granules into the nano-sized TiO_2 layer led to improve the light-harvesting efficiency due to the enhancement of light scattering. The highest efficiency (η = 6.51%) was achieved when the weight percentage of dispersed granules was 20 wt%, which was about 5.2% higher than that of the cell fabricated only by using TiO_2 nanoparticles. At 30 wt%, the cell efficiency was lower compared with the NP-based solar cell (0 wt%). According to the light absorbance spectra of photoanodes after the dye loading, the 30 wt% electrode showed the lower absorbance than the NP-based cell (0 wt%), indicating that the loading quantity of dye molecules is diminished. Given this, the decrease in the loading quantity of dye molecules at 30 wt% is main reason for the lower cell efficiency than the NP-based cell even though the light scattering is enhanced.

4. Conclusions

TiO_2 nanoparticles (NP) were synthesized by a hydrothermal method. The obtained TiO_2 nanoparticles had pure anatase phase and a rod-like shape with the average particle size of 10 to 30 nm depending on the hydrothermal temperature. According to the effect of hydrothermal temperature on the photovoltaic performance of DSSCs, the highest efficiency was achieved at the hydrothermal temperature of 200°C. TiO_2 granules (GP) of about 400 nm in average particle size were prepared by spray pyrolysis using the nanoparticles hydrothermally synthesized at 200°C. In terms of the light scattering, the GP-based photoanode was better than the NP-based electrode. But, the cell efficiency of the NP-based electrode was higher than the GP-based electrode because the dye-loading quantity and the recombination resistance were larger in the NP-based electrode than in the GP-based electrode. It was clear that the dispersion of GP into the nano-sized TiO_2 film enhances the light conversion efficiency. As a result, the cell efficiency of 6.51% was achieved for the electrode with the GP dispersion of 20 wt%. Compared with a pure NP film, the photo-conversion efficiency of the GP-dispersed photoanode was improved by 5.4% due to the enhancement of light scattering without the loss in the dye-loading quantity.

Acknowledgements

This research was supported by the research grant of the Korea Institute of Industrial Technology.

REFERENCES

[1] B. O'Regan, M. Grätzel, Nature **353**, 737 (1991).
[2] S.-W. Rhee, W. Kwon, Korean J. Chem. Eng. **28**, 1481 (2011).
[3] H. Alarcón, M. Hedlund, E.M.J. Johansson, H. Rensmo, A. Hagfeldt, G. Boschloo, J. Phys. Chem. C **111**, 13267 (2007).
[4] W. Liu, Z. Feng, W. Cao, Res. Chem. Intermed. **39**, 1623 (2013).
[5] M.M. Rashad, A.E. Shalan, M. Lira-Cantú, M.S.A. Abdel-Mottaleb, J. Ind. Eng. Chem. **19**, 2052 (2013).
[6] X. Zhu, H. Tsuji, A. Yella, A.-S. Chauvin, M. Gräzel, E. Nakamura, Chem. Commun. **49**, 582 (2013).
[7] S. Lee, Y. Jeon, Y. Lim, Md.A. Hossain, S. Lee, Y. Cho, H. Ju, W. Kim, Electrochim. Acta **107**, 675 (2013).
[8] A.C. Chandiran, A. Yella, M.T. Mayer, P. Gao, M.K. Nazeeruddin, M. Grätzel, Adv. Mater. **26**, 4309 (2014).
[9] L.-C. Chen, C.-R. Ke, J.-M. Ting, J. Electrochem. Soc. **161**, E28 (2014).
[10] J.Y. Ahn, K.J. Moon, J.H. Kim, S.H. Lee, J.W. Kang, H.W. Lee, S.H. Kim, Appl. Mater. Interfaces **6**, 903 (2014).
[11] W. Liu, Z. Feng, W. Cao, Res. Chem. Intermed. **39**, 1623 (2013).
[12] B.C. O'Regan, J.R. Durrant, P.M. Sommeling, N.J. Bakker, J. Phys. Chem. C **111**, 14001 (2007).
[13] S.-W. Lee, K.-S. Ahn, J. Phys. Chem. C **116**, 21285 (2012).
[14] T.T.T. Pham, T. Bessho, N. Mathews, S.M. Zakeeruddin, Y.M. Lam, S. Mhaisalkar, M. Grätzel, J. Mater. Chem. **22**, 16201 (2012).
[15] Y. Zhang, J. Zhang, P. Wang, G. Yang, Q. Sun, J. Zheng, Y. Zhu, Mater. Chem. Phys. **123**, 595 (2010).

Received: 20 November 2014.